A Morphological View of the Sodium 4,4′-Distyrylbiphenyl Sulfonate Fluorescent Brightness Distribution on Regenerated Cellulose Fibers

Eduardo T. Iamazaki,[1] Marcelo A. Pereira-Da-Silva,[2] Antonio J. F. Carvalho,[3] Rafaelle B. Romero,[1] Maria C. Gonçalves,[1] Teresa D. Z. Atvars[1]

[1]*Instituto de Química, Universidade Estadual de Campinas, Unicamp, Caixa Postal 6154, Campinas, SP 13084-971, Brazil*
[2]*Instituto de Física de São Carlos, Universidade de São Paulo, Caixa Postal 369, São Carlos, SP 13560-970, Brazil*
[3]*Universidade Federal de São Carlos, Caixa Postal 3031, Sorocaba, SP 18043-970, Brazil*

Received 19 May 2009; accepted 19 October 2009
DOI 10.1002/app.31670
Published online 22 June 2010 in Wiley InterScience (www.interscience.wiley.com).

ABSTRACT: Evidence of the sorption of the whitening agent sodium 4,4′-distyrylbiphenyl sulfonate in the presence of the anionic surfactant sodium dodecylsulfate or the cationic surfactant dodecyl trimethyl ammonium chloride on regenerated cellulose fibers is given by several microscopy techniques. Scanning electron microscopy provided images of the cylindrical fibers with dimensions of 3.5 cm (length) and 13.3 μm (thickness), with empty cores of 1 μm diameter and a smooth surface. Atomic force microscopy showed a fiber surface with disoriented nanometric domains using both tapping-mode height and phase image modes. Atomic force microscopy also showed that the whitening agent and surfactant molecules were sorbed onto the fiber surface, in agreement with the adsolubilization sorption model. Transmission electron microscopy showed fibers with nanometric parallel cylinders, surrounded by holes where the fluorescent whitening molecules accumulated. On the basis of these techniques, we conclude that the sorption process occurs preferentially on the fiber surface in contact with the water solution, and under saturated conditions, the whitening agent penetrates into the pores and are simultaneously sorbed on the pore walls bulk, forming molecular aggregates. © 2010 Wiley Periodicals, Inc. J Appl Polym Sci 118: 2321–2327, 2010

Key words: regenerated cellulose fibers; morphology; AFM; SEM; TEM; epifluorescence microscopy; FWA sorption

INTRODUCTION

Cellulose is a natural polymer composed of a syndiotactic polyacetal of glucose whose macromolecules are held together by intermolecular hydrogen bonds.[1,2] Their macromolecular chains have a polydisperse degree of polymerization.[1,2] Because of the hydrogen bonds, the supramolecular structure is described in terms of the degree of crystallinity and by the orientation and dimensions of the crystalline and amorphous regions.[3] The structure of fibers is morphologically organized according to several levels of ordering and sizes, which includes fibers, fibrils, and pores.[3–8] The unit cell of the crystalline phase is composed of cellulose units whose chains are attached by hydrogen bonds. Micelle fibrils are between 100 and 150 mers with parallel arrangements, a fibril unit is an association of 15 to 25 micellar microfibrils, and the fibrils are formed of 100 to 250 microfibrils.[3–7] On the other hand, fibers are randomly oriented in the amorphous regions.[3]

Regenerated cellulose fibers are widely used textile fibers whose properties depend on chemical composition, molar mass, degree of polymerization, degree of crystallinity, orientation of the crystallites, and processing conditions.[8–11] The surface charge of cellulose fibers is slightly negative due to the presence of carboxyl and hydroxyl groups,[6] and in particular, we determined that the regenerated cellulose fibers had a ζ-potential of −6.30 mV.[12] This small negative charge does not inhibited the sorption of a negative fluorescent whitening agent (FWA) such as the sodium 4,4′-distyrylbiphenyl sulfonate (Tinopal CBS) (Scheme 1), a stilbene-like molecule that absorbs in the UV region and emits in the visible region. Nevertheless, we also showed that the efficiency of the FWA sorption is strongly dependent on the presence of surfactants and on the surfactant concentration, and this process is favored when using cationic surfactant below its critical micelar concentration (cmc).[12–14] Similar results were reported for FWA sorption of whitening agent of cellulose fibers which indicated that an upper limit for

Additional Supporting Information may be found in the online version of this article.

Correspondence to: T. D. Z. Atvars (tatvars@iqm.unicamp.br).

Contract grant sponsors: FAPESP, CNPq, CAPES, MCT/CNPq/INEO.

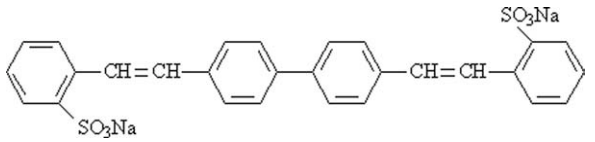

Scheme 1 Chemical structure of 4,4′-distyrylbiphenyl sodium sufonate salt (Tinopal CBS).

the whitening efficiency is achieved for higher loading sorption process.[15]

In earlier work, we determined quantitatively the amount of FWA sorption in regenerated cellulose fibers, and we established the role of the surfactant and salt on the efficiency of the sorption process.[12,13] However, because these papers focused on quantitative analyses of sorption processes, little information about the morphology of the fibers was presented. The aim of this work is to add a morphological view of the regenerated cellulose fibers sorbed with Tinopal CBS, which is the same FWA used in the other papers. Morphology was studied by scanning electron microscopy (SEM), transmission electron microscopy (TEM), atomic force microscopy (AFM), and epifluorescence microscopy in an attempt to describe the distribution of Tinopal on the fiber surface.

EXPERIMENTAL

Materials

Viscose fibers (from Vicunha Textile S.A., Brazil), sodium 4,4′-distyrylbiphenylsulfonate (Tinopal CBS, Sigma-Aldrich), sodium dodecyl sulfate (SDS) (Sigma, 98%), and dodecyltrimethylammonium chloride (DTAC) (Fluka, 97%) were used as received. For the FWA solutions, we used milli-Q purified water.

Viscose fibers (0.30 g) were dipped in 10 mL of Tinopal CBS aqueous solution (6×10^{-6} mol L^{-1}), with or without surfactants, in the absence of light for 20 min. Then, they were dried in an oven under a dynamic vacuum at $T = 35$°C for $\sim$ 24 h and stored in a desiccator. Other experimental details are described elsewhere.[12,13,16]

Methods

X-ray diffractrograms of a randomly oriented fiber bunch were recorded in the range of $2° < 2\theta < 50°$ on a Shimadzu-3A X-ray diffractrometer using a Cu Kα X-ray source ($\lambda = 1.54056$ Å) operating at 20 mA and 30 kV.

Differential scanning calorimetry (DSC) analysis was carried out in a TA Instruments MDSC 2910 Analyzer under a nitrogen atmosphere. A sample of about 10 μg was placed in the DSC pan. The sample was first stabilized at 25°C, and then it was heated to 250°C at a heating rate of 10°C/min.

For the scanning electron microscopy (SEM) experiments, regenerated cellulose fibers were carbon- and gold-coated by sputtering in a Bal-Tec MED 020 instrument. The sputtering chamber was under argon atmosphere ($P = 5 \times 10^{-2}$ mbar), maintained at low pressure by a turbo molecular pump and the target distance of 50 mm. The coating thickness was around 3 nm. The morphology of the fibers was examined in a Jeol JSM-6360LV scanning electron microscope, operating at an accelerating voltage of 20 kV, with a working distance of 10 mm. Magnification of 9000 and 7500× as indicated in the correspondent figures. Images were collected from the fiber surface and from the cryogenically fractured surface, giving information about the fiber dimensions, surface roughness, and fracture morphology.

Fibers for transmission electron microscopy (TEM) were embedded in a glycerol polyglycidyl ether resin (PELCO® Eponate 12) and sectioned with a Leica EM FC6 cryo-ultramicrotome at −120°C, using a diamond knife. Thin sections of the fibers (~50 nm thick) were examined with a Carl Zeiss CEM 902 transmission electron microscope, equipped with a Castaing-Henry energy filter spectrometer within the column. The images were recorded using a slow-scan CCD camera (Proscan) and processed in the iTEM Universal Imaging Platform.

Atomic force microscopy (AFM) experiments were performed with a Nanoscope®IIIa Multimode™ from Digital Instruments. The images were obtained under ambient conditions in the tapping mode. A commercial Si cantilever with a spring constant of 20 to 100 N/m was used, with free oscillation in the range between 250 and 300 kHz. Under these conditions, the tip fixed in the cantilever scans the fiber surface glued on a glass support. By measuring the deflections, the topology can be determined. Because

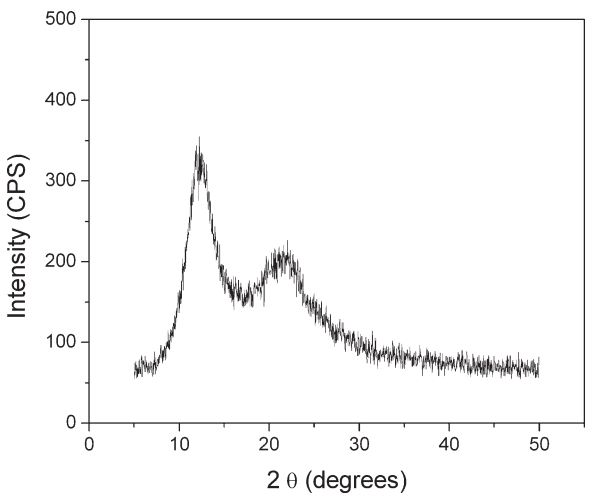

Figure 1 X-ray diffraction pattern of regenerated cellulose fibers.

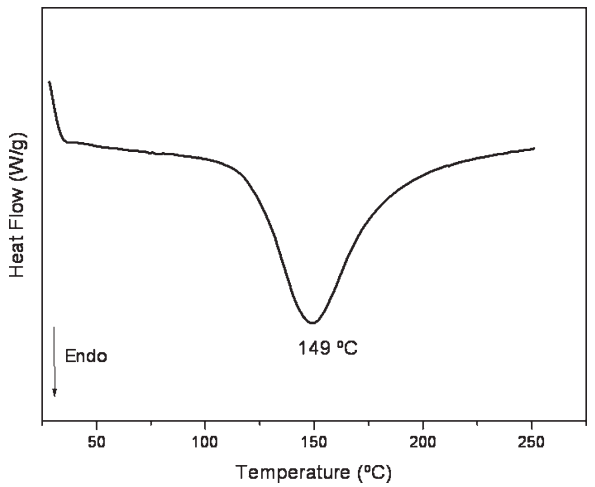

Figure 2 DSC curve for regenerated cellulose fibers.

of the curvature of the fiber surface, the lateral resolution of AFM imaging is limited.[7]

Steady-state fluorescence emission was recorded using an ISS PCI Photon spectrofluorimeter. These spectra were recorded from $\lambda_{em} = 370$ nm to $\lambda_{em} = 600$ nm with $\lambda_{exc} = 270$ nm, and the emission was collected by the back-face mode.

RESULTS AND DISCUSSION

Evidence of the presence of crystalline phases in these fibers was obtained from the X-ray diffraction pattern (Fig. 1), which shows two peaks: at $2\theta \sim 12.2^\circ$ and $2\theta \sim 21.7^\circ$. These peaks were assigned to the (110) and (200) indexes of the cellulose II type crystallites.[8,17] Additional evidence for the presence of crystalline phases in these fibers was obtained by DSC (Fig. 2), where an endothermic peak appears during sample heating at a peak temperature of 149°C.

Figure 3 shows the two SEM micrographs of regenerated cellulose fibers containg FWA (left side) and FWA+DTAC (right side). The fiber geometry is cylindrical with an average external diameter of 13 ± 1 μm on average, 3.5 ± 0.1 cm in length, with a smooth surface and a stripe in the longitudinal

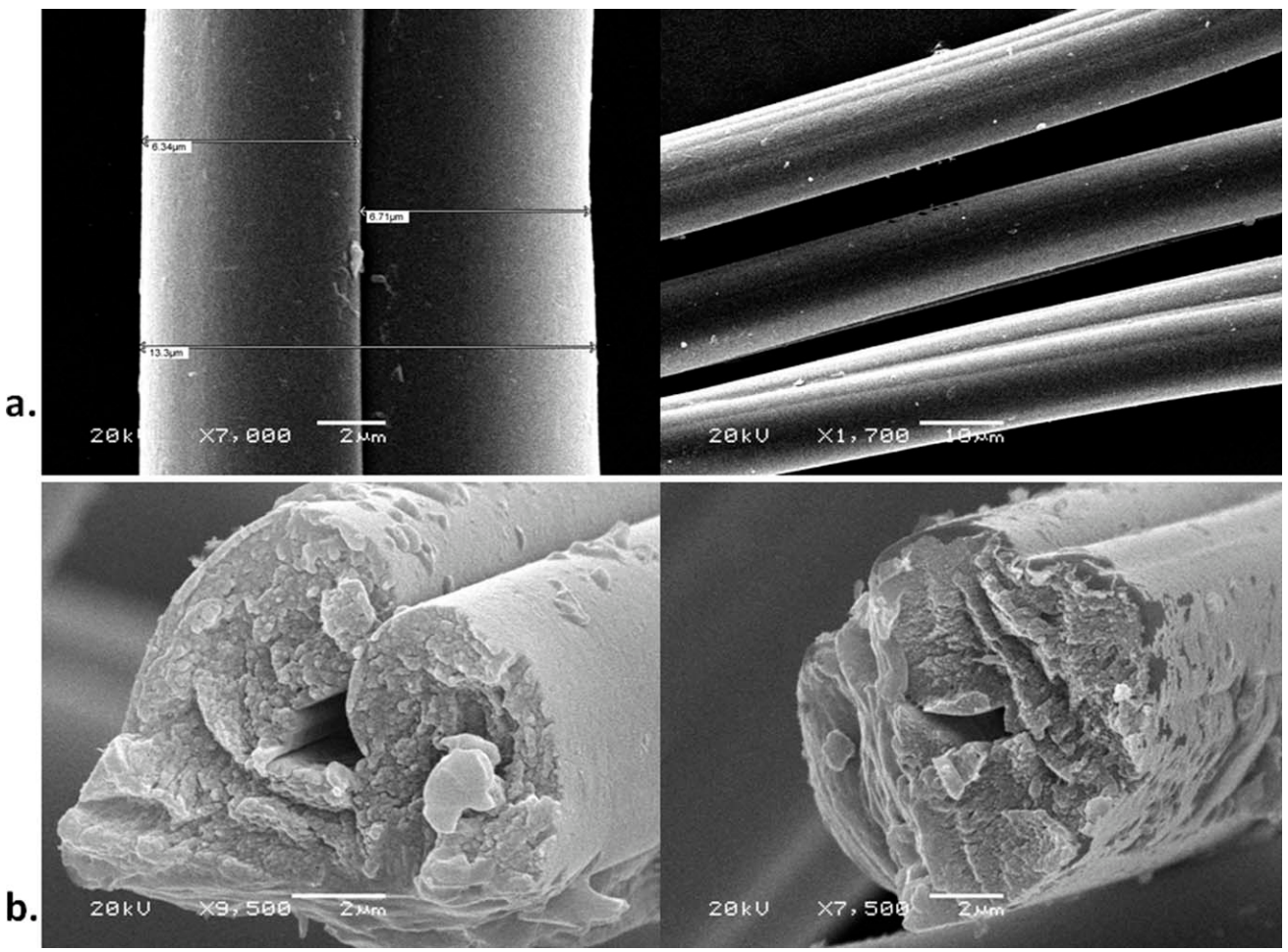

Figure 3 (a) SEM micrographs of a regenerated cellulose fiber produced by an extrusion process, with FWA sorbed on its surface (right side) and without FWA (left side); (b) Two SEM micrographs of the cryogenically fractured surface of a regenerated cellulose fiber with sorbed FWA, showing the "empty" central cavity in a glued and nonglued sheet.

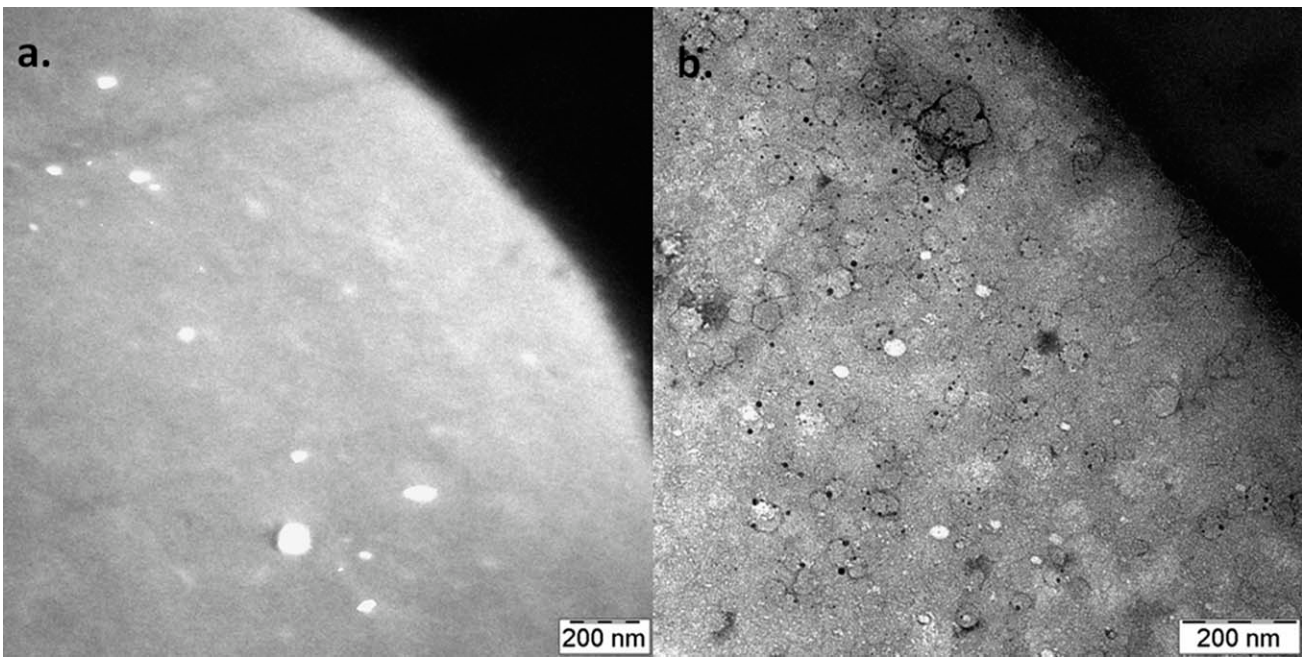

Figure 4 TEM micrographs of regenerated cellulose fiber cross sections: (a) original fiber and (b) fiber after Tinopal sorption. Bright domains are holes and dark regions correspond to aggregates of Tinopal.

direction. The shape is similar to a folded sheet in some cases and to an empty tube in others, and this is characteristic of regenerated cellulose fibers with high tenacity.[10] When FWA is sorbed in the presence of a surfactant, some clusters appeared on the fiber surface, as can be seen in Figure 3(a) (right side). Fibers with a tube shape also show an internal central hole with an average diameter of 1.1 μm, as observed by the SEM images of the surface after cryogenic fracture [Fig. 3(b)]. We can also see from the image of the fractured surface that the fiber is composed of a bunch of microfibrils, probably held together by hydrogen bonds.[3–5,7] Their shape is similar to a folded sheet. Some of these foils are glued together forming a closed cylinder (Fig. 3 right), some are not, forming an open tube (Fig. 3 left). These SEM micrographs give some details about the fiber morphology, show the presence of the surfactant, and/or FWA clusters, but no information about the distribution of either sorbed FWA or surfactant molecules could be obtained.

Evidence for the sorption of Tinopal onto the fibers was obtained initially by epifluorescence microscopy, which gives images that are dark under UV excitation without Tinopal (not shown) and blue and bright when Tinopal is present.[12] This has also been demonstrated by fluorescence spectroscopy, where the emission of Tinopal sorbed on the fiber has a well-resolved vibronic structure[12,13] and by the brightness, whiteness, and yellowness determinations.[18] These data showed that compared with the standard (fiber without Tinopal), fibers whitened in the presence of SDS have more brightness, more whiteness, and less yellowness, and these appear to be independent of the SDS concentration; those in the presence of DTAC (cationic surfactant) had greater brightness and whiteness and less yellowness. Moreover, the efficiency is higher when the concentration reaches the DTAC cmc, between 10 and 15 mmol $L^{-1,}$ but is practically independent of the SDS concentration.[12,13] These results are explained by the adsolubilization model, where both the surfactant and Tinopal are being competitively sorbed onto the fiber.[19–21] If this is true, we expect that images of clusters of surfactant should be observed by electron microscopy.

Real space observations of the morphological characteristics of the fibers on the nanometric scale were investigated by transmission electron microscopy (TEM) (Fig. 4). In the absence of Tinopal [Fig. 4(a)], the cellulosic network structure is uniform throughout the cross section, except for the presence of some brighter domains, probably associated with the presence of cellulose microfibrils. In addition, we observed some voids with dimensions ranging from 10 to 80 nm, indicating that the fibers are not completely dense.

The micrographs of the regenerated cellulose fibers treated with FWA exhibit some differences only when saturated with Tinopal. They show well-defined circular domains, defined by dark boundaries of Tinopal and dark nanodomains of Tinopal aggregates [Fig. 4(b)]. The improvement in contrast with TEM may be caused by the higher concentration of Tinopal, which is a sodium sulfonic salt. This result demonstrates that the FWA dispersion is not

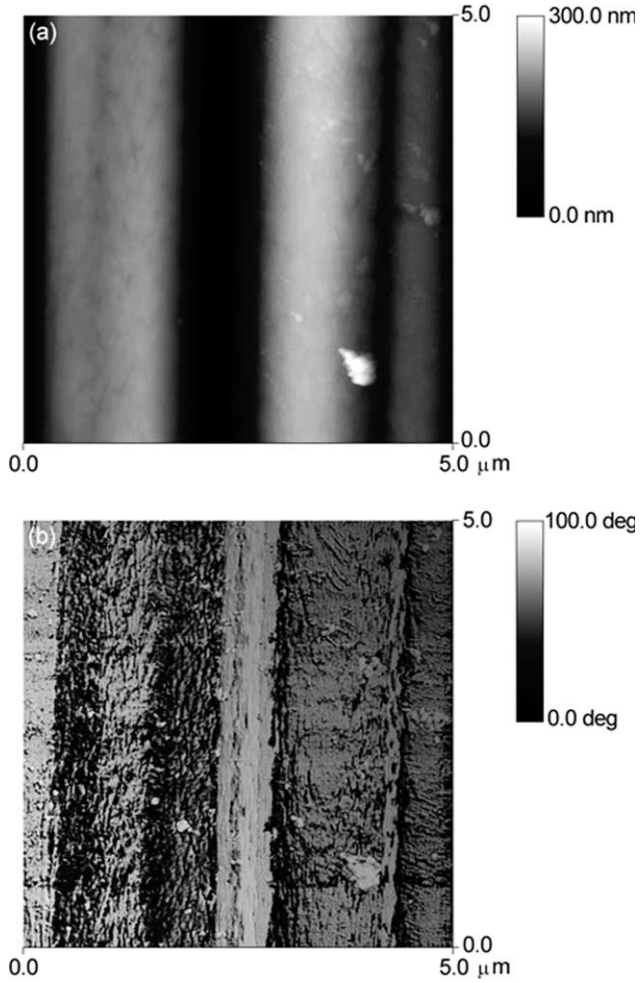

Figure 5 AFM (a) tapping-mode height image and (b) tapping-mode phase image of regenerated cellulose fiber surface without FWA.

completely uniform with higher concentrations, although the epifluorescence images seem to be uniform. Actually, a uniform distribution of dyes into semicrystalline polymer matrices is not expected, because the dye molecules do not promptly penetrate into the crystalline domains.[21,22] We can also observe in Figure 4(b) that the external surface of the fiber, which is in direct contact with the solution during the sorption process, is darker, which provides additional evidence for the sorption of Tinopal molecules. These domains have also been observed by SEM [Fig. 3(a)] and were attributed to the orientation of the crystalline phase of the regenerated cellulose fiber along the extrusion direction.

Further details of the morphology of the regenerated cellulose fiber surface were obtained using AFM in both tapping and phase modes. For fibers without Tinopal, the images using AFM tapping-mode height [Fig. 5(a)] give a topological view of the fiber surface, where the dark strip corresponds to the region where the folded foil is glued, and the brighter region corresponds to the curved surface of the fiber cylinder. A smooth surface on the nanometric scale is observed in agreement with the topological view shown by SEM in Figure 3(a). On the other hand, phase contrast images recorded in intermittent contact can give information on such properties as viscoelasticity or stiffness, since energy dissipation reflects mainly the mechanical behavior of the sample surface. The phase image presented in Figure 5(b) shows the presence of crystalline nanodomains formed by the alignment of the macromolecular chains during fiber processing.

AFM images of the fiber surface with a high concentration of sorbed Tinopal using the tapping-mode [Fig. 6(a)] also show a smooth surface on the nanometric scale. As for native fibers [Fig. 5(a)], the central vein is also observed in the longitudinal direction. The phase image [Fig. 6(b)] shows oriented domains at nanoscale dimensions with a different texture compared with the native fibers [Fig. 5(b)]: globular domains are observed for fibers containing a high concentration of Tinopal, suggesting that,

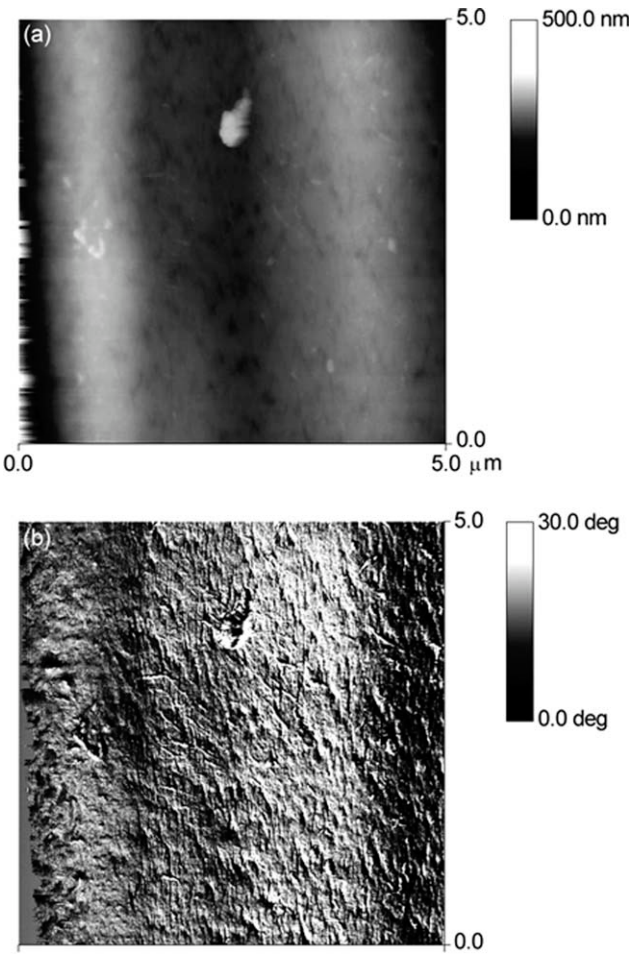

Figure 6 AFM (a) tapping-mode height image and (b) tapping-mode phase image of regenerated cellulose fiber surface with sorbed Tinopal.

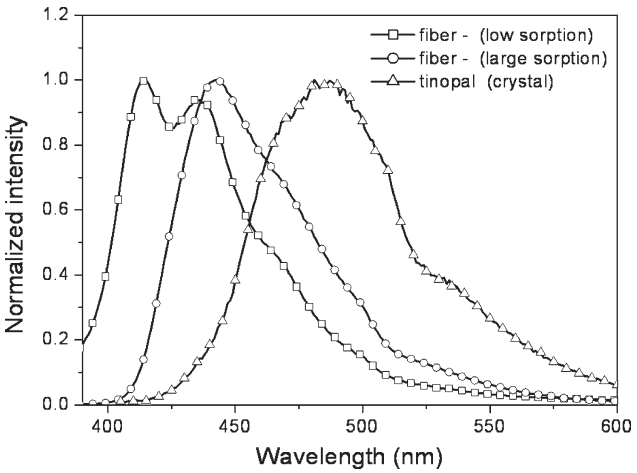

Figure 7 Normalized fluorescence spectra of Tinopal in: (Δ) crystalline phase, (○) sorbed into fibers at higher sorption yield, and (□) sorbed into fibers at lower sorption yield. $\lambda_{exc} = 348$ nm.

under these conditions, Tinopal might undergo an aggregation process. Additional figures of AFM tapping-mode height topography images of the regenerated natural fiber and those with sorbed Tinopal are shown in the Supporting Information Figures 1 and 2.

Additional evidence for Tinopal aggregation was obtained by fluorescence spectroscopy. The fluorescence spectrum of Tinopal aggregates is different from the emission of isolated molecules.[12,13] As shown in Figure 7, the fluorescence spectrum of crystallized Tinopal is broad and centered at 486 nm, and that of Tinopal sorbed into the fibers at a higher sorption yield is also broad and centered at 443 nm. The spectrum of Tinopal/fiber at a lower sorption yield is vibronically structured with two well-resolved peaks at 414 nm and 435 nm. Thus, although the emission of aggregates is not similar to that of Tinopal in its crystalline phase, the spectrum does not resemble the emission of a completely solvated molecule, either in dilute solution or sorbed at a lower concentration onto the fiber. This red-shift of the emission spectrum of the aggregates is responsible for the yellowing appearence of the fiber under higher loading conditions, introducing a deteriorating effect on the whitening process. This is known as photoyellowing of the textile fibers. Moreover, this effect is more important for solutions containing DTAC, as a higher loading sorption process was obtained.

Different AFM images were also produced when Tinopal was sorbed from an aqueous solution containing the surfactants DTAC and SDS (Figs. 8 and 9, respectively) in concentrations equal to the cmc. In both cases, the fiber surface becomes smoother with the presence of globular aggregates, visible as lighter domains in the tapping-mode height images [Figs. 8(a) and 9(a)]. These domains have a polydisperse size distribution: the size range is larger for the Tinopal/DTAC system (from 30 nm to 300 nm) than for the Tinopal/SDS system, which is in the range from 15 to 70 nm. The AFM tapping-mode height topography images of the fiber surface after the sorption of Tinopal in the presence of a cationic surfactant (DTAC) and of an anionic surfactant (SDS) are shown in the Supporting Information Figures 3 and 4, respectively.

Considering that the regenerated cellulose fibers used in all the experiments belong to the same bath, only the type of surfactant was changed, the only possible explanation for the differences seen must be attributed to fiber/surfactant and Tinopal/surfactant interactions. In accordance with the adsolubilization model,[19,20] we assume that because DTAC and the fiber have opposite charges, there is an initial electrostatic interaction between the surfactant head and the fiber surface when the surfactant concentration is low, and they are preferentially sorbed. Bilayers are formed at intermediate concentration relatively

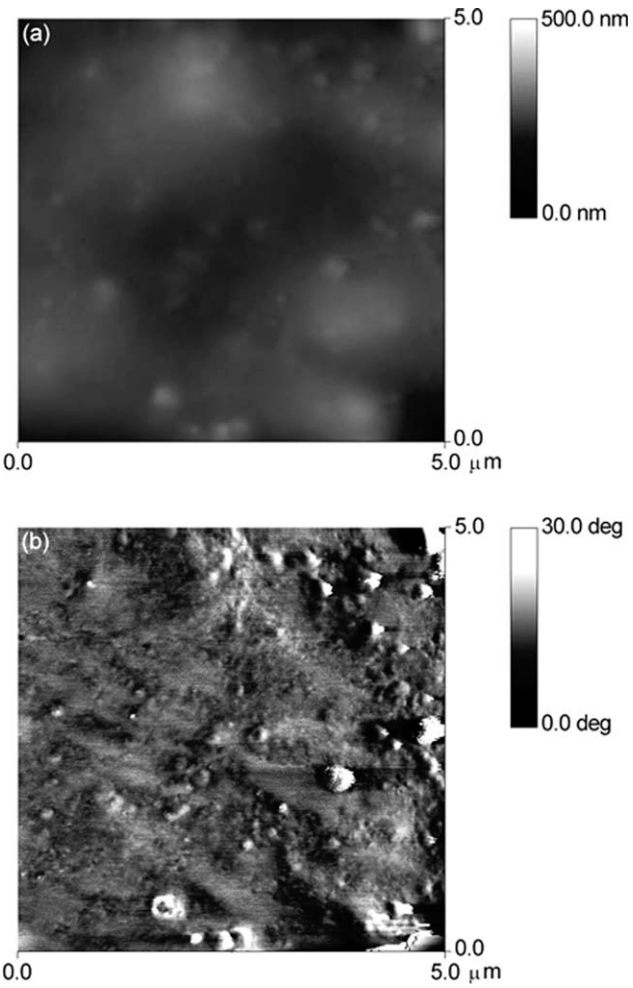

Figure 8 AFM (a) tapping-mode height image and (b) tapping-mode phase image of regenerated cellulose fiber surface with Tinopal sorbed in the presence of DTAC.

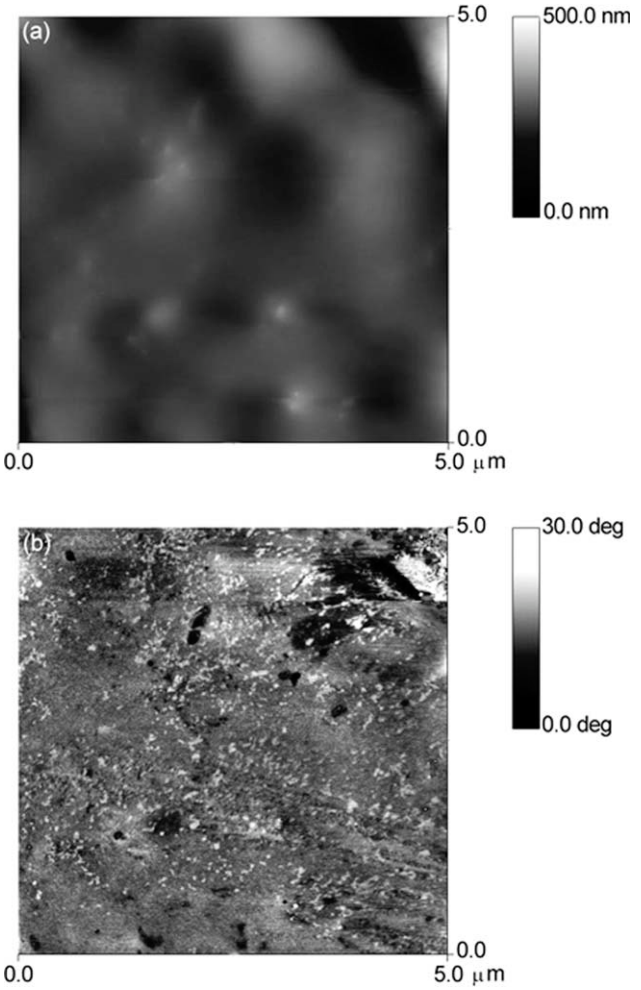

Figure 9 AFM (a) tapping-mode height image and (b) tapping-mode phase image of regenerated cellulose fiber surface with Tinopal sorbed in the presence of SDS.

to the surfactant cmc, and surfactant micelles are formed at concentrations higher than the cmc. Larger concentrations of Tinopal are sorbed in the two initial stages, which suggest that Tinopal is sorbed simultaneously with the surfactant, probably induced by the electrostatic interaction involving the opposite charges of the positive head of the surfactant and the negative charge of Tinopal. On the other hand, the system that has negative SDS/Tinopal also undergoes sorption on the fibers, although in a lower amount and with smaller micelles. Both processes are induced by the presence of counterions. Therefore, the circular domains observed in the AFM images are probably surfactant micelles, in addition to Tinopal aggregates.

CONCLUSIONS

This report describes the morphology of regenerated cellulose fibers with sorbed Tinopal CBS, a FWA. Fibers as received have smooth surfaces. When they contain Tinopal, from an optical point of view, the FWA is uniformly distributed onto the fiber surface and in the bulk, and a strong blue emission can be generated by UV-irradiation. The fiber morphology obtained by scanning electron microscopy and transmission electron microscopy indicates that the fibers have a smooth surface, with the bulk being formed by bunches of fibrils and holes. Tinopal can only be detected by TEM when very high concentrations are used. In this case, Tinopal aggregates are seen on the surface of the microfibrils. We can also see a relatively higher concentration of Tinopal on the fiber surface in the region that is in close contact with the aqueous solution. The morphological characterization of the Tinopal/fiber system can be obtained by AFM, which yields images that indicate that Tinopal effectively covered the fiber surface. In the presence of a surfactant, micelles can also be observed.

The authors thank Prof. Carol Collins for useful discussions.

References

1. Pielesz, A.; Wesełucha-Birczyńska, A.; Freeman, H. S.; Włochowicz, A. Cellulose 2005, 12, 497.
2. Kreze, T.; Strand, S.; Stana-Kleinschek, K.; Ribitsch, V. Mater Res Innov 2001, 4, 107.
3. Abu-Rous, M.; Ingolic, E.; Schuster, K. C. Cellulose 2006, 13, 411.
4. Jakob, H. F.; Fengel, D.; Tschegg, S. E.; Fratzl, P. Macromolecules 1995, 28, 8782.
5. Há, M. A.; Apperley, D. C.; Evans, B. W.; Huxham, M.; Jardine, W. G.; Vietor, R. J.; Reis, D.; Vian, B.; Jarvis, M. C. Plant J 1998, 16, 183.
6. Muller, M.; Hori, R.; Itoh, T.; Sugiyama, J. Biomacromolecules 2002, 3, 182.
7. Nigmatullin, R.; Lovitt, R.; Wright, C.; Linder, M.; Nakari-Setala, T.; Gama, A. Colloids Surf B Biointerfaces 2004, 35, 125.
8. Zugenmaier, P. Prog Polym Sci 2001, 26, 1341.
9. Krassig, H. Tappi 1978, 61, 93.
10. Kotek, R. In Handbook of Fiber Chemistry, 3rd ed.; Lewin, M., Ed.; CRC Press: New York, 2007; p 667.
11. Mikhailov, N. V.; Gorbacheva, V. O.; Krasova, I. I.; Milkova, L. P.; Bochkina, V. S.; Nikolaeva, N. S. Fiber Chem 1972, 2, 619.
12. Iamazaki, E. T.; Atvars, T. D. Z. Langmuir 2007, 23, 12886.
13. Iamazaki, E. T.; Atvars, T. D. Z. Langmuir 2006, 22, 9866.
14. Stana-Kleinschek, K.; Strand, S.; Ribitsch, V. Polym Eng Sci 1999, 39, 1412.
15. Stana-Kleinschek, K.; Pohar, C.; Ribitsch, V. Colloid Polym Sci 1995, 273, 1174.
16. Yamaki, S. B.; Barros, D. S.; Garcia, C. M.; Socoloski, P.; Oliveira, O. N.; Atvars, T. D. Z. Langmuir 2005, 21, 5414.
17. Kim, J.; Yun, S.; Ounaies, Z. Macromolecules 2006, 39, 4202.
18. Iamazaki, E. T.; Atvars, T. D. Z. Dyes Pigm 2008, 76, 669.
19. Aloulou, F.; Boufi, S.; Belgacem, N.; Gandini, A. Colloid Polym Sci 2004, 283, 344.
20. Alila, S.; Boufi, S.; Belgacem, M. N.; Beneventi, D. Langmuir 2005, 21, 8106.
21. O'Haver, J. H.; Harwell, J. H. In Surfactant Adsorption and Surface Solubilization. ACS Symposium Series 615; Sharma, R., Ed.; American Chemical Society: Washington, 1995; p 49.
22. Talhavini, M.; Atvars, T. D. Z.; Schurr, O.; Weiss, R. G. Polymer 1998, 39, 3221.